Telecom Networking with a Diamond Quantum Memory

Eric Bersin,[1,2,*,†] Madison Sutula,[3,†] Yan Qi Huan,[3] Aziza Suleymanzade,[3] Daniel R. Assumpcao,[4] Yan-Cheng Wei,[3] Pieter-Jan Stas,[3] Can M. Knaut,[3] Erik N. Knall,[4] Carsten Langrock,[5] Neil Sinclair,[4] Ryan Murphy,[1] Ralf Riedinger,[3,6,7] Matthew Yeh,[4] C.J. Xin,[4] Saumil Bandyopadhyay,[2] Denis D. Sukachev,[3,8] Bartholomeus Machielse,[3,8] David S. Levonian,[3,8] Mihir K. Bhaskar,[3,8] Scott Hamilton,[1] Hongkun Park,[3,9] Marko Lončar,[4] Martin M. Fejer,[5] P. Benjamin Dixon,[1] Dirk R. Englund,[2] and Mikhail D. Lukin[3]

[1] *Lincoln Laboratory, Massachusetts Institute of Technology, Lexington, Massachusetts 02421, USA*

[2] *Department of Electrical Engineering and Computer Science, Massachusetts Institute of Technology, Cambridge, Massachusetts 02139, USA*

[3] *Department of Physics, Harvard University, Cambridge, Massachusetts 02138, USA*

[4] *John A. Paulson School of Engineering and Applied Sciences, Harvard University, Cambridge, Massachusetts 02138, USA*

[5] *E. L. Ginzton Laboratory, Stanford University, Stanford, California 94305, USA*

[6] *Institut für Laserphysik und Zentrum für Optische Quantentechnologien, Universität Hamburg, Hamburg 22761, Germany*

[7] *The Hamburg Centre for Ultrafast Imaging, Hamburg 22761, Germany*

[8] *AWS Center for Quantum Networking, Boston, Massachusetts 02135, USA*

[9] *Department of Chemistry and Chemical Biology, Harvard University, Cambridge, Massachusetts 02138, USA*

(Received 31 July 2023; accepted 15 December 2023; published 8 January 2024)

Practical quantum networks require interfacing quantum memories with existing channels and systems that operate in the telecom band. Here we demonstrate low-noise, bidirectional quantum frequency conversion that enables a solid-state quantum memory to directly interface with telecom-band systems. In particular, we demonstrate conversion of visible-band single photons emitted from a silicon-vacancy (SiV) center in diamond to the telecom O band, maintaining low noise ($g^2(0) < 0.1$) and high indistinguishability ($V = 89 \pm 8\%$). We further demonstrate the utility of this system for quantum networking by converting telecom-band time-bin pulses, sent across a lossy and noisy 50-km deployed fiber link, to the visible band and entangling them with a diamond quantum memory with fidelity $\mathcal{F} \geq 87 \pm 2.5\%$. These results demonstrate the viability of SiV quantum memories integrated with telecom-band systems for scalable quantum networking applications.

DOI: 10.1103/PRXQuantum.5.010303

Many promising applications of quantum information systems [1–4] require the ability to transmit quantum states over long distances. Quantum memories with efficient, high-fidelity photon interfaces are a crucial enabling technology for long-distance quantum communication. They can serve as quantum network nodes, enabling single-photon generation [5], realization of quantum repeaters [6–8], and deterministic quantum operations between photonic qubits [9]. While most promising quantum memories operate in the visible band, standard communication infrastructure typically operates in the telecom band, designed for compatibility with existing communication channels such as low-loss deployed fibers. For these reasons, the realization of interfaces between visible-band quantum systems and telecom-band classical systems is crucial for development of practical, networked quantum systems. Accordingly, interfaces for converting between visible and telecom wavelengths, generating entanglement between quantum memories and converted telecom photons, and memory-memory entanglement mediated by converted telecom photons have been explored for a number of prominent quantum memories, including trapped ions [10,11], neutral atoms

*Eric.Bersin@ll.mit.edu

†These authors contributed equally to this work.

[12–14], solid-state color centers [15,16], and quantum dots [17].

Here, we combine low-noise quantum frequency conversion (QFC) with a diamond silicon-vacancy (SiV) center coupled to a nanophotonic cavity to realize a system for telecom-band networking of a solid-state quantum memory. We demonstrate that this scheme can operate bidirectionally: first, we show that single photons generated by an SiV can be converted to 1350 nm while preserving their quantum properties. Next, we demonstrate that time-bin qubits generated at 1350 nm and subsequently converted to match the SiV's optical transition can be entangled with the SiV electron spin with high-fidelity, a resource for heralded state transfer.

In QFC, an input quantum field is overlapped with a strong pump field (frequency ω_p) inside of a nonlinear material, shifting the frequency of the input while otherwise preserving its quantum properties [18]. This is often performed as depicted in Fig. 1(a), using difference (sum)-frequency generation in a $\chi^{(2)}$ material such as periodically poled lithium niobate (PPLN) to achieve frequency down- (up-) conversion between visible (ω_v) and telecom (ω_t) frequencies. While such nonlinear frequency conversion is routinely employed in classical applications for the production of coherent radiation at novel wavelengths or for detecting long-wavelength signals, in quantum applications, noise photons from spontaneous parametric down-conversion (SPDC) and Raman scattering [19,20] generated by the strong pump field (typically 100-mW class) lower the resulting fidelity of the transduced quantum state [21]. At frequencies below the pump frequency $\omega_t < \omega_p$, Stokes Raman and SPDC processes result in a broadband noise plateau, whereas at higher frequencies $\omega_t > \omega_p$, the comparatively weaker anti-Stokes Raman signal typically tapers off for separations $\Delta\omega_{tp} = \omega_t - \omega_p > 30$ THz [22]. This leads to two noise regimes—one lower-noise, anti-Stokes regime where $\omega_p < \omega_t$, and one higher-noise, Stokes and SPDC-dominated regime where $\omega_p > \omega_t$. Since ω_v is fixed by the choice of quantum memory, conservation of energy $\omega_p = \omega_v - \omega_t$ restricts the design of QFC schemes to only one degree of freedom. Moreover, the need for a strong pump laser introduces an additional engineering consideration due to availability of common gain materials. The resulting trade space

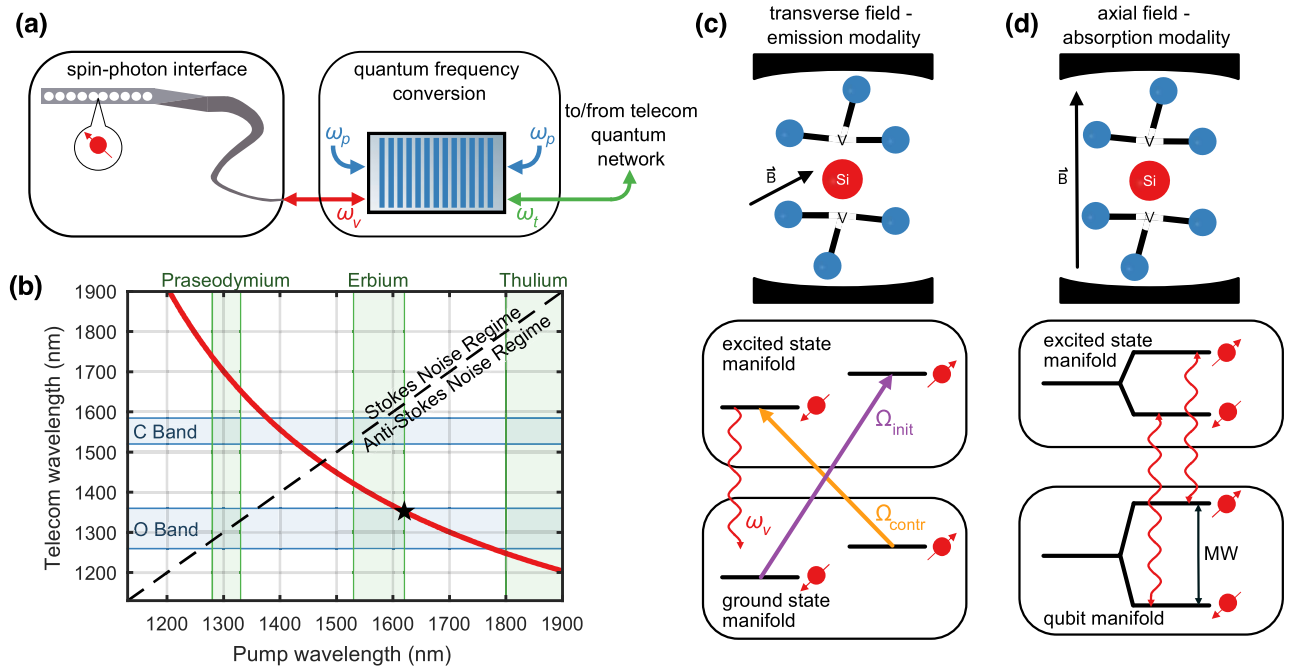

FIG. 1. (a) Quantum networks based on a spin-photon interface with a single atomlike defect center such as silicon-vacancy centers in diamond coupled to a nanophotonic cavity. Such memories often exhibit visible emission frequencies ω_v, necessitating quantum frequency conversion (QFC) to a telecom frequency ω_t mediated by a pump at ω_p. (b) The parameter space for low-noise QFC using a single $\chi^{(2)}$-based conversion step. The red line indicates conversion schemes that can be performed for the SiV's 737-nm transition, the blue shaded regions indicate the low-loss telecom O and C bands, and green shaded regions indicate what conversion processes can be easily pumped given common gain materials. The black star indicates our conversion scheme. (c) SiV emission modality: an SiV in an overcoupled cavity and a transverse external magnetic field can be driven coherently with alternating initialization (Ω_{init}) and control optical pulses (Ω_{contr}) to emit single photons near 737 nm (ω_v). (d) SiV absorption modality: an SiV in a critically coupled cavity and an axial external magnetic field exhibits spin-conserving optical transitions that yield spin-dependent cavity reflectivity, enabling entanglement with an incoming photonic qubit at ω_v.

[Fig. 1(b)] permits selection of a frequency conversion scheme based on the desired telecom wavelength, the noise requirements of the application, and the availability of pump laser amplifiers.

The negatively charged diamond SiV center is a promising candidate for the realization of quantum networks. Its solid-state nature enables on-chip integration and packaging [23–25], its electronic spin degree of freedom can store quantum information over millisecond timescales at dilution refrigerator temperatures [26] or single-Kelvin temperatures when strained [27], and its optical transition exhibits nearly lifetime-limited spectral stability due to its inversion-symmetric electronic structure [28]. This stability permits integration into nanophotonic crystal cavities, which provide an efficient interface for spin-photon state transduction. For example, as shown in Fig. 1(c), an overcoupled photonic crystal cavity enhances emission of the incorporated SiV into the desired optical mode. Under an applied transverse magnetic field, the SiV exhibits allowed transitions between spin states that can be driven to initialize the spin state via optical pumping, or to generate high-quality, shaped single photons [29]. This "emission modality" is a resource for quantum networking or quantum photonic processing applications, which benefit from sources of high-quality single photons [30]. Alternatively, an SiV can operate in an "absorption modality" when incorporated into a critically coupled photonic crystal cavity and placed in an axial magnetic field as shown in Fig. 1(d) [31]. This results in spin-dependent cavity reflectivity that can be used to generate entanglement with a reflected time-bin photonic qubit.

The SiV's 737-nm optical transition wavelength at which these protocols operate experiences strong loss in standard single-mode optical fiber (>5 dB/km), necessitating QFC to a low-loss telecom band. Examining the trade-space curve corresponding to the SiV in Fig. 1(b), we identify a point (black star) where a long-wavelength pump at 1623 nm facilitates conversion to the edge of the O band at 1350 nm (typical loss approximately 0.3 dB/km in standard single-mode telecom fiber), permitting operation in the lower-noise anti-Stokes regime. This point maximizes $\Delta\omega_{tp}$ within the parameter space in order to minimize pump-induced noise. See Supplemental Material [32] (as well as Refs. [33–35] therein) for a similar analysis using other emerging quantum memories, as well as with multipump conversion schemes [16,36,37]. Transmitting quantum signals at 1350 nm offers an additional advantage when co-propagating quantum signals alongside classical telecommunication signals, which typically occupy the C band around 1530–1565 nm. This large spectral separation allows for efficient and high-extinction separation of quantum and classical data, preventing cross-talk noise that can degrade protocol fidelity [38].

Figure 2(a) depicts our experimental setup for generating and converting single photons using a SiV center incorporated in an overcoupled photonic crystal cavity, following the approach used in Ref. [29]. A tapered optical fiber is coupled to the device to deliver optical control

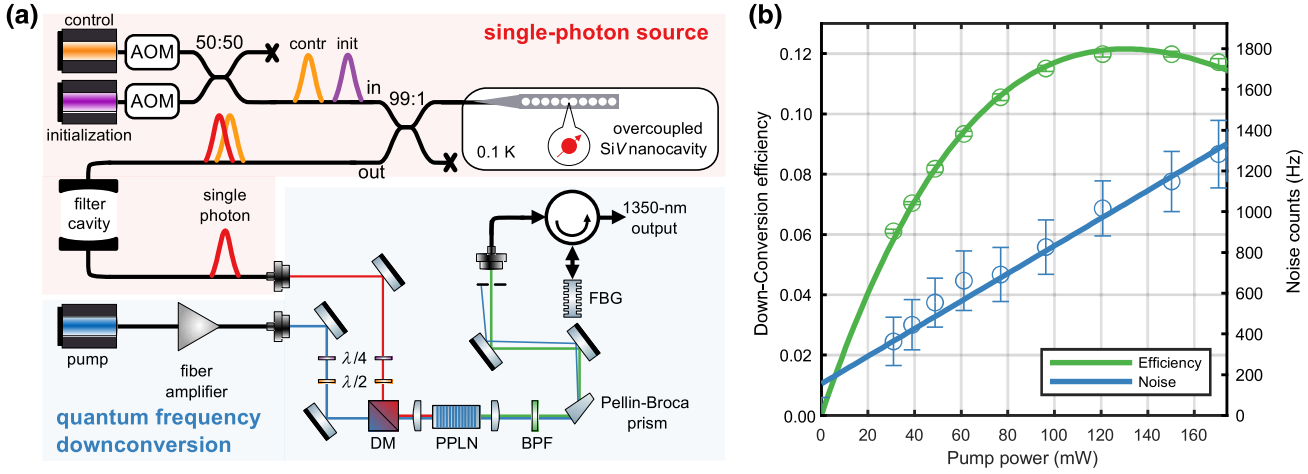

FIG. 2. (a) An SiV in emission modality is driven to produce single photons near 737 nm, which are efficiently collected by an overcoupled nanophotonic cavity then filtered from the driving fields with a free-space Fabry-Pérot cavity before being sent to a frequency down-conversion setup. A pump laser at 1623 nm is amplified by a fiber amplifier (BKtel photonics) then coupled to free space. Half- and quarter-wave plates on both the pump and signal paths optimize coupling into the TE mode of the PPLN waveguide. The pump and signal are overlapped on a dichroic mirror (DM) and coupled into the PPLN waveguide where conversion occurs. The converted output is collected and filtered by a 25-nm-bandwidth bandpass filter (BPF), a Pellin-Broca prism, and ultimately a 50-GHz filter formed by a circulator and fiber Bragg grating (FBG). (b) Total external conversion efficiency (green) measured using a classical 737-nm input, and pump-induced noise (blue) as a function of pump power inside the PPLN waveguide. The noise shown here is calculated for the output of the conversion setup, accounting for the efficiency and dark counts of our SNSPDs.

pulses, as well as to efficiently collect single photons. We apply optical control pulses to produce a shaped single-photon output with a temporal width of 30 ns at a repetition rate of 670 kHz. A Fabry-Pérot filter removes residual optical excitation light from the emitted photons, resulting in a final single photon generation efficiency of $\eta = 5.0 \pm 0.1\%$ within a 75-ns collection window.

Next, we convert these single photons to the telecom O band using a custom-fabricated PPLN waveguide device (see Supplemental Material [32] as well as Ref. [39] therein). Our input fields are a pump laser at 1623 nm amplified by a fiber amplifier and a 737-nm signal, either from a laser for QFC efficiency characterization, or from the output of our SiV emission setup for single-photon conversion experiments. An aspheric lens couples both fields into separate waveguide modes of the PPLN, where an on-chip wavelength division multiplexer (WDM) combines the two modes. The PPLN waveguide output is collimated by a second aspheric lens, and residual pump light is removed by a 25-nm bandpass filter followed by a Pellin-Broca prism with a pinhole after 40 cm of propagation length. Finally, the converted light is sent through a fine filter setup comprising a circulator and a 50-GHz-bandwidth fiber Bragg grating to remove broadband anti-Stokes Raman noise.

In the strong-pump limit, the total external conversion efficiency is dependent on the pump power in the waveguide P and the length of the interaction region L [40]:

$$\eta_{\text{ext}} = \eta_{\text{opt}}\eta_{\text{int}} \sin^2\left(L\sqrt{\eta_0 P}\right), \tag{1}$$

where η_{opt} is the combined efficiency of all optical components and filtering, η_{int} is the maximum internal conversion efficiency of the PPLN, and η_0 is the normalized internal efficiency, which is determined by the nonlinear material, mode overlap, etc. We measure $\eta_{\text{opt}} \approx 19\%$, limited by coupling losses between the crystal waveguide mode and optical fiber (32% total) and the fiber Bragg filter (59%). By measuring the maximum depletion of the input 737-nm signal, we estimate an internal efficiency $\eta_{\text{int}} \approx 65\%$. This conversion is maximized at an internal pump power of approximately 130 mW, which for our interaction length $L = 35$ mm indicates a normalized internal efficiency $\eta_0 \approx 1.54 \times 10^4\ \text{W}^{-1}\ \text{m}^{-2}$. Sweeping the pump power [Fig. 2(b)] and fitting the 1350-nm output power to Eq. (1) shows a maximum conversion efficiency of $\eta_{\text{ext}} = 12.2 \pm 0.1\%$, consistent with the losses described above. This overall efficiency is within a factor of 3 to 4 of leading demonstrations [11,13,14,21] limited by our waveguide coupling and device efficiency, both of which could be improved to the state of the art by further device optimization [32,41].

We probe the noise generated by the strong pump by measuring the setup output on superconducting nanowire single-photon detectors (SNSPDs) with zero 737-nm input power, plotted in Fig. 2(b) after correction for the SNSPD detection efficiency and dark counts. The noise profile fits to a linear dependency of 6.8 ± 0.9 Hz/mW of noise photons generated by the pump, indicating anti-Stokes Raman scattering is the primary source. This noise reaches a count rate of 1.0 ± 0.1 kHz when the conversion efficiency is at its maximum. Due to the broadband nature of this pump-induced noise, a useful metric is the noise spectral density at maximum conversion $\rho = 21 \pm 2$ Hz/GHz, which compares favorably to other systems designed for diamond defect centers [42] and indicates the ultimate fidelity limits for a QFC system given optimal filtering.

We characterize our QFC system's ability to preserve quantum states by measuring the second-order correlations of the single-photon output. First, we benchmark our single-photon source at its native visible wavelength, finding good single-photon character of $g^2(0) = 0.0092 \pm 0.0002$ without background or detector dark-count subtraction [Fig. 3(a)]. Next, we convert these single photons to the telecom O band, then send them through a 0.1-km-long fiber network (69% efficient) between two buildings before detection on SNSPDs (29% efficient). During the single-photon conversion experiments, we measure a mean QFC efficiency of $6 \pm 2\%$, attributing the additional loss and high variance compared to the classical case to polarization drift in the fibers between the SiV and our QFC setup. As a result, the SNR within our 75-ns gated time bins is 14.5 ± 0.1. For the converted photons, we measure $g^{(2)}(0) = 0.090 \pm 0.025$, again without background or detector dark-count subtraction [Fig. 3(b)], indicating good preservation of quantum properties through QFC.

The quantum properties of our converted photons can be further probed via Hong-Ou-Mandel interference between subsequent SiV emissions, using a 1-km delay line as shown in Fig. 3. A polarization controller in the short arm of the resultant interferometer permits us to adjust the relative polarizations between the two arms and compare between the distinguishable case, where the photons arriving from both arms at the final beam splitter are cross-polarized [Fig. 3(c)], and the indistinguishable case, where the photons arriving at the final beam splitter are co-polarized [Fig. 3(d)]. We measure a HOM interference visibility $V = 1 - g^{(2)}_{\parallel}(0)/g^{(2)}_{\perp}(0) = 89 \pm 8\%$.

We next demonstrate that our scheme is compatible with absorption-based quantum memory protocols by performing frequency up-conversion on a telecom-wavelength qubit. Figure 4(a) depicts our experimental setup for generating telecom time-bin photonic qubits, upconverting them to match the SiV's visible transition, and generating spin-photon entanglement. For this experiment, we use an SiV in a critically coupled photonic crystal cavity [27] and an axial magnetic field, resulting in spin-dependent cavity reflectivity that can be used to generate entanglement with a reflected time-bin photonic qubit.

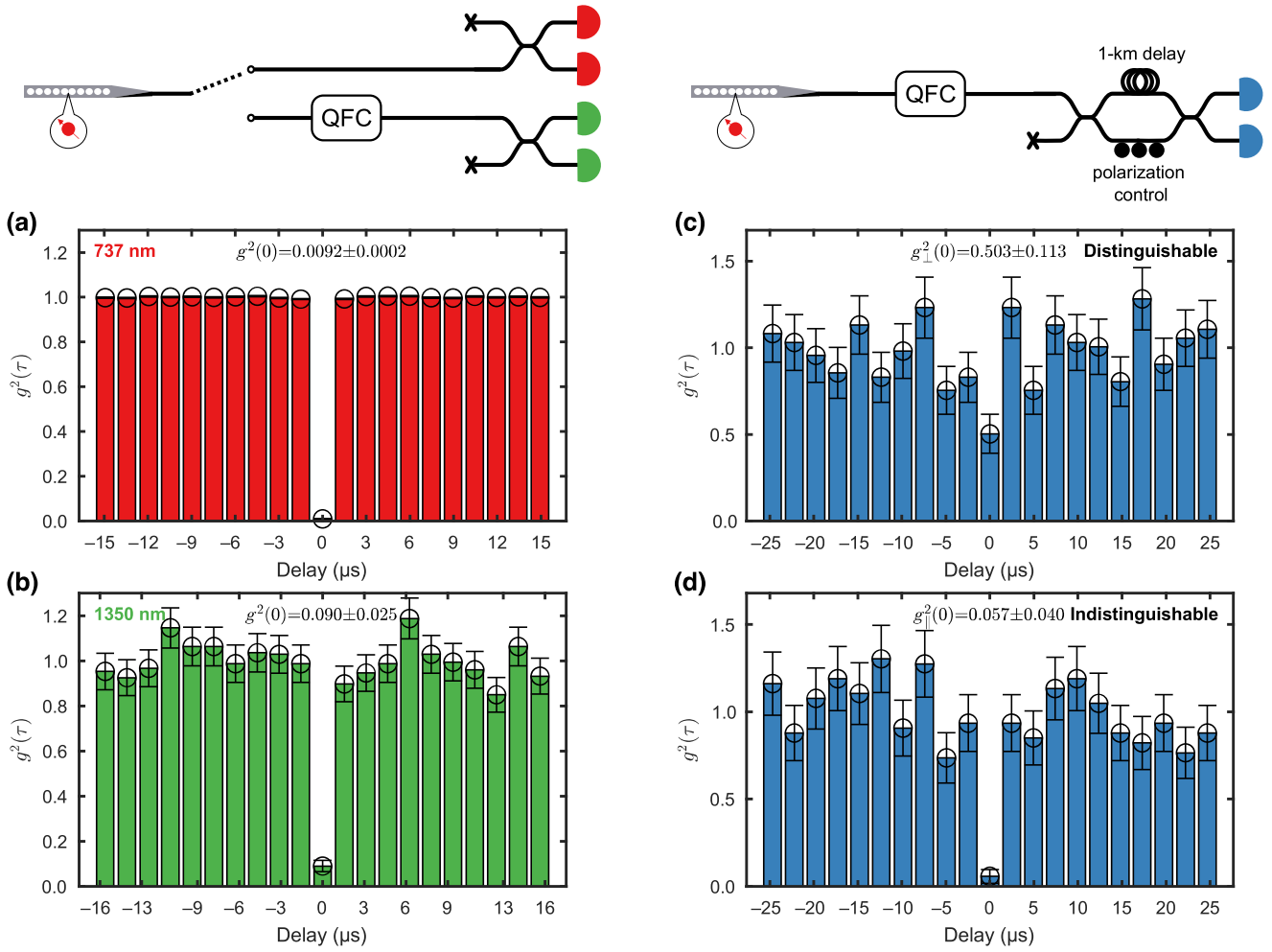

FIG. 3. Hanbury Brown-Twiss (HBT) interferometry of single photons emitted by an SiV (a) before and (b) after frequency down-conversion, without correction for background noise or detector dark counts. In spite of the noise induced by the frequency converter due to our modest filtering, the $g^2(0)$ remains below 0.1, indicating strong single-photon quality. We further perform Hong-Ou-Mandel (HOM) interferometry between successive emissions of the SiV using a 1-km delay line, with a polarization controller in one arm of the delay line to compare between (c) distinguishable and (d) indistinguishable cases. The resultant visibility is measured to be 89 ± 8%, in line with expectations from the background noise. In all plots, the error bars correspond to the normalized standard deviation due to shot noise.

We use a 1350 nm laser to generate coherent time-bin pulses with a full-width at half-maximum of 45 ns and separated by 144.5 ns. These pulses are generated at MIT Lincoln Laboratory in Lexington, MA, 15.4 km away from the QFC receiver at Harvard University in Cambridge, MA. A 50 km deployed fiber link connects the two sites and attenuates the pulses by 33.7 dB such that they ultimately arrive at the SiV device as qubits with mean photon number $\langle\hat{n}\rangle \approx 0.1$ per pulse. This channel also imparts noise associated with deployed fiber communications, including polarization drift, timing drift, and Doppler shifts. To coordinate between the two sites, we co-propagate a 1550 nm clock signal which synchronizes the experiment between the two sites, as well as a periodic 1350 nm reference signal to correct for polarization drifts over the deployed fiber and to serve as a reference for any drift in the photonic qubit's optical frequency. Details about the link as well as our classical communications protocol for synchronization and stabilization can be found in Ref. [43].

We modify our QFC setup from Fig. 2(a) to upconvert light from 1350 to 737 nm via sum-frequency generation using an identically fabricated PPLN device. Compared to the previous setup, we replace the lenses and filters to be wavelength appropriate, and propagate the optical fields in reverse through the PPLN so that the on-chip WDM is at the output rather than the input. Importantly, the increased spectral separation between the pump and converted wavelength for up-conversion relaxes our filtering requirements, such that the converted light is only filtered by a 13-nm-bandwidth bandpass filter and a prism, without any fine filtering stage. As shown in Fig. 4(b), we are

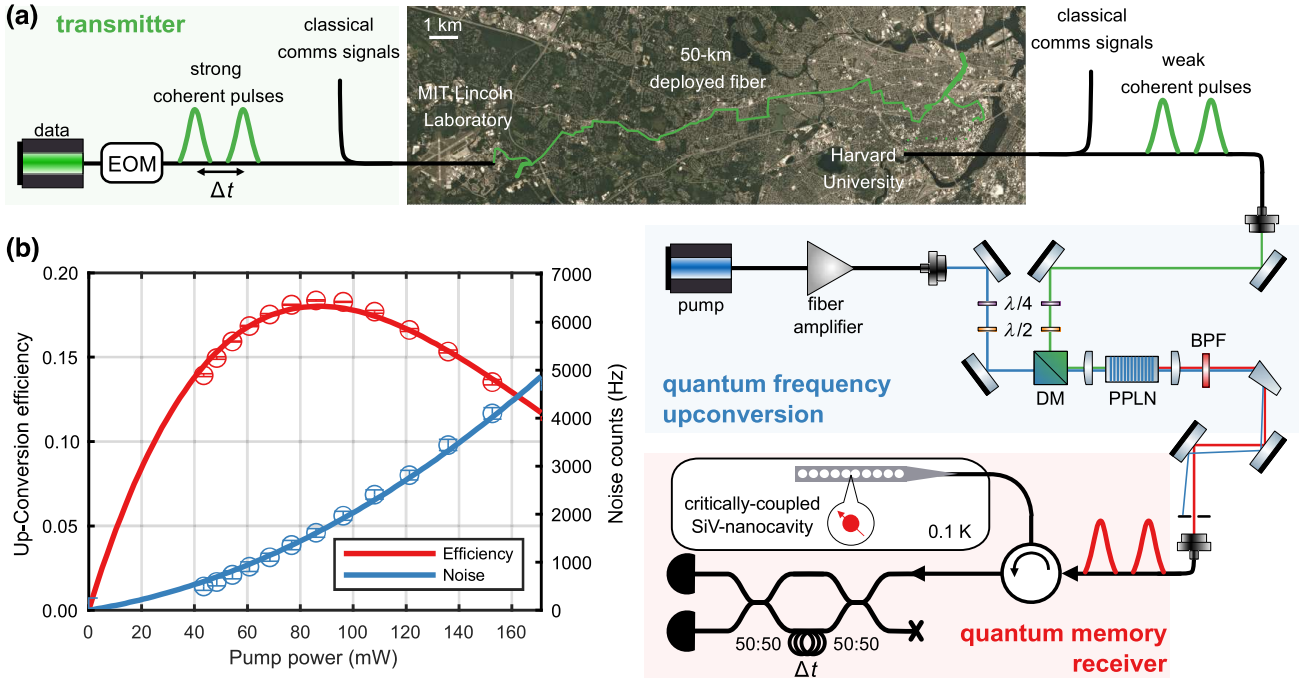

FIG. 4. (a) A 1350-nm data laser located at MIT Lincoln Laboratory is carved into time-bin pulses, multiplexed with signals for classical communications, then sent over a 50-km fiber link (green path: solid line exact route, dashed line approximate), which attenuates these pulses by 33.7 dB and adds environmental noise associated with deployed fiber. These data pulses are sent to a frequency up-conversion setup designed similarly to the setup for down-conversion [Fig. 2(a)], but without the narrow final FBG filter. The resultant visible time-bin qubits are sent through a circulator and reflected off an SiV in absorption modality. Reflected light is collected and measured on a time-delay interferometer, heralding protocol success. (b) The relaxed filtering requirements permit an increased conversion efficiency of $18 \pm 0.2\%$, while maintaining a low noise count rate of 1.6 ± 0.03 kHz.

thus able to attain an increased conversion efficiency of $18.0 \pm 0.2\%$ while maintaining a low noise count rate of 1.63 ± 0.03 kHz after correcting for detector dark counts. We note that here, the noise profile fits well to a quadratic power dependency, suggesting these noise counts are dominated by up-conversion of anti-Stokes photons rather than direct Raman noise [22]. The output of the conversion setup is sent through a fiber-optic circulator and delivered via a tapered fiber to the SiV cavity, where light is transmitted or reflected depending on the SiV spin state. Reflected light is routed to a time-delay interferometer (TDI) that measures the photonic qubit using avalanche photodiodes. Using this system and the pulse sequence shown in Fig. 5(a), we generate the spin-photon entangled state $|\psi\rangle = (|E\downarrow\rangle + |L\uparrow\rangle)/\sqrt{2}$ conditioned on successful detection of a reflected photon. Here, $|E\rangle$ and $|L\rangle$ denote the presence of a photon in an early or late time bin, respectively. We characterize this entanglement by measuring the photon and the spin in the joint ZZ and XX bases. Figure 5(b) shows the retrieved spin-photon correlations, limited primarily by residual reflectivity of the $|\downarrow\rangle$ state [32]. Following Ref. [44], we use these correlations to calculate an entanglement fidelity of $\mathcal{F} \geq 87.0 \pm 2.5\%$; we note that this is a lower bound, taken without correcting for readout errors. This result constitutes a heralded transduction protocol that reveals no information about the absorbed state, providing a key resource for quantum repeaters and other quantum networking protocols.

Taken together, these experiments demonstrate bidirectional quantum interface between a diamond quantum memory and telecom photons. In particular, the SiV's 737-nm transition wavelength and our choice of conversion between the telecom O band enabled the use of a long-wavelength pump, reducing the noise induced by the conversion process. Our heralded state transduction from a telecom photon to a diamond memory, incorporating classical telecommunication signals for timing synchronization and stabilization over deployed fiber, highlights the compatibility of the SiV platform with telecommunication infrastructure. This work can be extended and improved along several directions. The conversion efficiency was limited by coupling losses and nonunity internal conversion efficiency, and could be improved by further device optimization to realize up to $\eta_{\text{ext}} \approx 70\%$ [41]. Our down-conversion demonstration utilized a broad filter over $100\times$ the SiV's lifetime limited linewidth; using a narrower final filter thus offers a clear avenue for further SNR improvement. While our protocol fidelity was limited by the finite cooperativity of the device used here (max $C \sim 1.6$), other works have shown

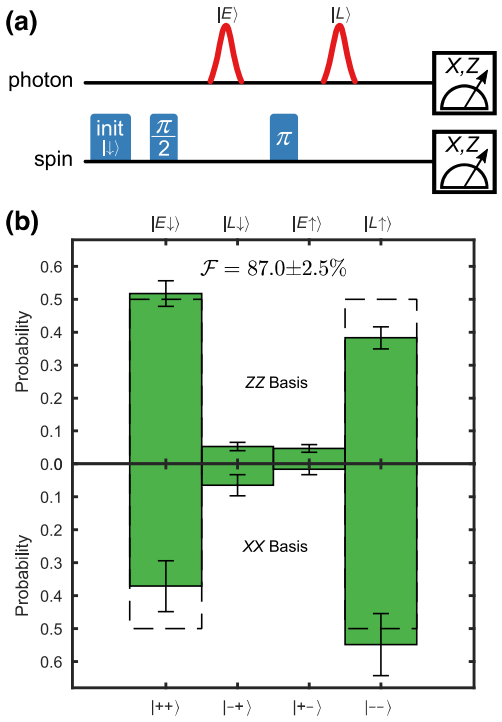

FIG. 5. (a) Pulse sequence for generating and verifying photonic state transduction. (b) Fidelity of the spin-photon entanglement. Measurement of a transmitted photon in the X basis heralds protocol success, whereupon the spin is read out in the X or Z basis, as appropriate for the photon state sent.

higher cooperativities $C > 100$, enabling higher fidelities $\mathcal{F} > 94\%$ [45].

The ability to transduce single-photon quantum states between visible and telecom wavelengths with high fidelity has implications across quantum information science applications. Single telecom photons are an important resource for photonic quantum computing; replacing current resource state generators with single telecom photon sources would improve processing efficiency and reduce errors from multiphoton events [29,46–50]. Furthermore, our system can be used for generating multiphoton entangled states when interfaced with a second cavity-coupled SiV [45]. When used as an input to a photonic processor, such cluster states can dramatically improve the efficiency and fidelity of photonic quantum computers [5]. When combined with access to nuclear memories [27] and improved nanophotonic devices, these results offer a path towards more general deployed quantum networking. The high-bandwidth nature of our conversion system [32] enables bridging of the frequency difference between individual SiVs due to the natural inhomogeneous distribution [51–53], and provides an avenue for taking advantage of the built-in spectral multiplexing of solid-state memories [54]. This approach also allows for interfacing SiVs with other quantum information platforms such as neutral atoms [35], trapped ions [10,55], or other color centers in diamond [56,57], where performing frequency conversion to a common wavelength would facilitate photonic-mediated entanglement generation between these systems. This could enable quantum networks comprising diverse physical qubits, where different applications including computing, communication or sensing could be performed by physical systems best tailored to the task.

ACKNOWLEDGMENTS

This material is based upon work supported by the National Reconnaissance Office and the Under Secretary of Defense for Research and Engineering under Air Force Contract No. FA8702-15-D-0001. Any opinions, findings, conclusions or recommendations expressed in this material are those of the authors and do not necessarily reflect the views of the National Reconnaissance Office or the Under Secretary of Defense for Research and Engineering.

We thank Catherine Lee, David Starling, Franco Wong, and Ian Christen for helpful discussions. This work was supported by the National Science Foundation (NSF, Grant No. PHY-2012023), NSF EFRI ACQUIRE (Grant No. 5710004174), NSF QuIC-TAQS (Grant No. OMA-2137723), Center for Ultracold Atoms (Grant No. PHY-1734011), Department of Energy (DoE, Grant No. DESC0020115), AFOSR MURI (Grants No. FA9550171002 and No. FA95501610323), and Center for Quantum Networks (Grant No. EEC-1941583). Devices were fabricated at the Harvard Center for Nanoscale Systems, NSF Award No. 1541959. E.B. and M.S. acknowledge funding from a NASA Space Technology Research Fellowship. Y.Q.H. acknowledges support from the Agency for Science, Technology and Research (A*STAR) National Science Scholarship. D.A., E.N.K., and B.M. acknowledge support by the NSF Graduate Research Fellowship under Grant No. DGE1745303. M.Y. acknowledges funding from the Department of Defence (DoD) through the National Defense Science and Engineering Graduate (NDSEG) Fellowship Program. R.R. acknowledges support by the Alexander von Humboldt Foundation, the Cluster of Excellence "Advanced Imaging of Matter" of the Deutsche Forschungsgemeinschaft (DFG)—EXC 2056—Project ID 390715994, BMBF Project 16KIS1592K. We thank Planet.com for allowing us to take custom satellite imagery.

[1] Daniel Gottesman, Thomas Jennewein, and Sarah Croke, Longer-baseline telescopes using quantum repeaters, Phys. Rev. Lett. **109**, 070503 (2012).

[2] E. T. Khabiboulline, J. Borregaard, K. De Greve, and M. D. Lukin, Quantum-assisted telescope arrays, Phys. Rev. A **100**, 022316 (2019).

[3] Feihu Xu, Xiongfeng Ma, Qiang Zhang, Hoi-Kwong Lo, and Jian-Wei Pan, Secure quantum key distribution with realistic devices, Rev. Mod. Phys. **92**, 025002 (2020).

[4] H. J. Kimble, The quantum internet, Nature **453**, 1023 (2008).

[5] Netanel H. Lindner and Terry Rudolph, Proposal for pulsed on-demand sources of photonic cluster state strings, Phys. Rev. Lett. **103**, 113602 (2009).

[6] H.-J. Briegel, W. Dür, J. I. Cirac, and P. Zoller, Quantum repeaters: The role of imperfect local operations in quantum communication, Phys. Rev. Lett. **81**, 5932 (1998).

[7] W. J. Munro, K. A. Harrison, A. M. Stephens, S. J. Devitt, and Kae Nemoto, From quantum multiplexing to high-performance quantum networking, Nat. Photonics **4**, 792 (2010).

[8] S. L. N. Hermans, M. Pompili, H. K. C. Beukers, S. Baier, J. Borregaard, and R. Hanson, Qubit teleportation between non-neighbouring nodes in a quantum network, Nature **605**, 663 (2022).

[9] I. Schwartz, D. Cogan, E. R. Schmidgall, Y. Don, L. Gantz, O. Kenneth, N. H. Lindner, and D. Gershoni, Deterministic generation of a cluster state of entangled photons, Science **354**, 434 (2016).

[10] Matthias Bock, Pascal Eich, Stephan Kucera, Matthias Kreis, Andreas Lenhard, Christoph Becher, and Jürgen Eschner, High-fidelity entanglement between a trapped ion and a telecom photon via quantum frequency conversion, Nat. Commun. **9**, 1998 (2018).

[11] V. Krutyanskiy, M. Meraner, J. Schupp, V. Krcmarsky, H. Hainzer, and B. P. Lanyon, Light-matter entanglement over 50 km of optical fibre, npj Quantum Inf. **5**, 72 (2019).

[12] Rikizo Ikuta, Toshiki Kobayashi, Tetsuo Kawakami, Shigehito Miki, Masahiro Yabuno, Taro Yamashita, Hirotaka Terai, Masato Koashi, Tetsuya Mukai, Takashi Yamamoto, and Nobuyuki Imoto, Polarization insensitive frequency conversion for an atom-photon entanglement distribution via a telecom network, Nat. Commun. **9**, 1997 (2018).

[13] Tim van Leent, Matthias Bock, Robert Garthoff, Kai Redeker, Wei Zhang, Tobias Bauer, Wenjamin Rosenfeld, Christoph Becher, and Harald Weinfurter, Long-distance distribution of atom-photon entanglement at telecom wavelength, Phys. Rev. Lett. **124**, 010510 (2020).

[14] Xi-Yu Luo, Yong Yu, Jian-Long Liu, Ming-Yang Zheng, Chao-Yang Wang, Bin Wang, Jun Li, Xiao Jiang, Xiu-Ping Xie, Qiang Zhang, Xiao-Hui Bao, and Jian-Wei Pan, Postselected entanglement between two atomic ensembles separated by 12.5 km, Phys. Rev. Lett. **129**, 050503 (2022).

[15] Anaïs Dréau, Anna Tchebotareva, Aboubakr El Mahdaoui, Cristian Bonato, and Ronald Hanson, Quantum frequency conversion of single photons from a nitrogen-vacancy center in diamond to telecommunication wavelengths, Phys. Rev. Appl. **9**, 064031 (2018).

[16] Marlon Schäfer, Benjamin Kambs, Dennis Herrmann, Tobias Bauer, and Christoph Becher, Two-stage, low noise quantum frequency conversion of single photons from silicon-vacancy centers in diamond to the telecom c-band, Adv. Quantum Technol. **2023**, 2300228 (2023).

[17] Jonas H. Weber, Benjamin Kambs, Jan Kettler, Simon Kern, Julian Maisch, Hüseyin Vural, Michael Jetter, Simone L. Portalupi, Christoph Becher, and Peter Michler, Two-photon interference in the telecom c-band after frequency conversion of photons from remote quantum emitters, Nat. Nanotechnol. **14**, 23 (2019).

[18] Prem Kumar, Quantum frequency conversion, Opt. Lett. **15**, 1476 (1990).

[19] J. S. Pelc, C. Langrock, Q. Zhang, and M. M. Fejer, Influence of domain disorder on parametric noise in quasi-phase-matched quantum frequency converters, Opt. Lett. **35**, 2804 (2010).

[20] Sebastian Zaske, Andreas Lenhard, and Christoph Becher, Efficient frequency downconversion at the single photon level from the red spectral range to the telecommunications c-band, Opt. Express **19**, 12825 (2011).

[21] Anna Tchebotareva, Sophie L. N. Hermans, Peter C. Humphreys, Dirk Voigt, Peter J. Harmsma, Lun K. Cheng, Ad L. Verlaan, Niels Dijkhuizen, Wim de Jong, Anaïs Dréau, and Ronald Hanson, Entanglement between a diamond spin qubit and a photonic time-bin qubit at telecom wavelength, Phys. Rev. Lett. **123**, 063601 (2019).

[22] J. S. Pelc, L. Ma, C. R. Phillips, Q. Zhang, C. Langrock, O. Slattery, X. Tang, and M. M. Fejer, Long-wavelength-pumped upconversion single-photon detector at 1550 nm: Performance and noise analysis, Opt. Express **19**, 21445 (2011).

[23] Noel H. Wan, Tsung-Ju Lu, Kevin C. Chen, Michael P. Walsh, Matthew E. Trusheim, Lorenzo De Santis, Eric A. Bersin, Isaac B. Harris, Sara L. Mouradian, Ian R. Christen, Edward S. Bielejec, and Dirk Englund, Large-scale integration of near-indistinguishable artificial atoms in hybrid photonic circuits, Nature **583**, 226 (2019).

[24] David J. Starling, Katia Shtyrkova, Ian Christen, Ryan Murphy, Linsen Li, Kevin C. Chen, Dave Kharas, Xingyu Zhang, John Cummings, W. John Nowak, Eric Bersin, Robert J. Niffenegger, Madison Sutula, Dirk Englund, Scott Hamilton, and P. Benjamin Dixon, Fully packaged multi-channel cryogenic quantum memory module, Phys. Rev. Appl. **19**, 064028 (2023).

[25] Beibei Zeng, Chawina De-Eknamkul, Daniel Assumpcao, Dylan Renaud, Zhuoxian Wang, Daniel Riedel, Jeonghoon Ha, Carsten Robens, David Levonian, Mikhail Lukin, Ralf Riedinger, Mihir Bhaskar, Denis Sukachev, Marko Loncar, and Bart Machielse, Cryogenic packaging of nanophotonic devices with a low coupling loss <1 dB, Appl. Phys. Lett. **123**, 161106 (2023).

[26] D. D. Sukachev, A. Sipahigil, C. T. Nguyen, M. K. Bhaskar, R. E. Evans, F. Jelezko, and M. D. Lukin, Silicon-vacancy spin qubit in diamond: A quantum memory exceeding 10 ms with single-shot state readout, Phys. Rev. Lett. **119**, 223602 (2017).

[27] P.-J. Stas, Y. Q. Huan, B. Machielse, E. N. Knall, A. Suleymanzade, B. Pingault, M. Sutula, S. W. Ding, C. M. Knaut, D. R. Assumpcao, Y.-C. Wei, M. K. Bhaskar, R. Riedinger, D. D. Sukachev, H. Park, M. Lončar, D. S. Levonian, and M. D. Lukin, Robust multi-qubit quantum network

node with integrated error detection, Science **378**, 557 (2022).

[28] A. Sipahigil, K. D. Jahnke, L. J. Rogers, T. Teraji, J. Isoya, A. S. Zibrov, F. Jelezko, and M. D. Lukin, Indistinguishable photons from separated silicon-vacancy centers in diamond, Phys. Rev. Lett. **113**, 113602 (2014).

[29] E. N. Knall, C. M. Knaut, R. Bekenstein, D. R. Assumpcao, P. L. Stroganov, W. Gong, Y. Q. Huan, P.-J. Stas, B. Machielse, M. Chalupnik, D. Levonian, A. Suleymanzade, R. Riedinger, H. Park, M. Lončar, M. K. Bhaskar, and M. D. Lukin, Efficient source of shaped single photons based on an integrated diamond nanophotonic system, Phys. Rev. Lett. **129**, 053603 (2022).

[30] Pieter Kok, W. J. Munro, Kae Nemoto, T. C. Ralph, Jonathan P. Dowling, and G. J. Milburn, Linear optical quantum computing with photonic qubits, Rev. Mod. Phys. **79**, 135 (2007).

[31] C. T. Nguyen, D. D. Sukachev, M. K. Bhaskar, B. Machielse, D. S. Levonian, E. N. Knall, P. Stroganov, R. Riedinger, H. Park, M. Lončar, and M. D. Lukin, Quantum network nodes based on diamond qubits with an efficient nanophotonic interface, Phys. Rev. Lett. **123**, 183602 (2019).

[32] See Supplemental Material http://link.aps.org/supplemental/10.1103/PRXQuantum.5.010303.

[33] Matthew E. Trusheim *et al.* Transform-limited photons from a coherent tin-vacancy spin in diamond, Phys. Rev. Lett. **124**, 023602 (2020).

[34] Xiyuan Lu, Gregory Moille, Ashutosh Rao, and Kartik Srinivasan, Proposal for noise-free visible-telecom quantum frequency conversion through third-order sum and difference frequency generation, Opt. Lett. **46**, 222 (2021).

[35] Tim van Leent, Matthias Bock, Florian Fertig, Robert Garthoff, Sebastian Eppelt, Yiru Zhou, Pooja Malik, Matthias Seubert, Tobias Bauer, Wenjamin Rosenfeld, Wei Zhang, Christoph Becher, and Harald Weinfurter, Entangling single atoms over 33 km telecom fibre, Nature **607**, 69 (2022).

[36] Vahid Esfandyarpour, Carsten Langrock, and Martin Fejer, Cascaded downconversion interface to convert single-photon-level signals at 650 nm to the telecom band, Opt. Lett. **43**, 5655 (2018).

[37] J. Hannegan, U. Saha, J. D. Siverns, J. Cassell, E. Waks, and Q. Quraishi, C-band single photons from a trapped ion via two-stage frequency conversion, Appl. Phys. Lett. **119**, 084001 (2021).

[38] Ben Amies-King, Karolina P. Schatz, Haofan Duan, Ayan Biswas, Jack Bailey, Adrian Felvinti, Jaimes Winward, Mike Dixon, Mariella Minder, Rupesh Kumar, Sophie Albosh, and Marco Lucamarini, Quantum communications feasibility tests over a uk-ireland 224-km undersea link, Entropy. **25**, 1572 (2023).

[39] M. L. Bortz, S. J. Field, M. M. Fejer, D. W. Nam, R. G. Waarts, and D. F. Welch, Noncritical quasi-phase-matched second harmonic generation in an annealed proton-exchanged $LiNbO_3$ waveguide, IEEE J. Quantum. Electron. **30**, 2953 (1994).

[40] Rostislav V. Roussev, Carsten Langrock, Jonathan R. Kurz, and M. M. Fejer, Periodically poled lithium niobate waveguide sum-frequency generator for efficient single-photon detection at communication wavelengths, Opt. Lett. **29**, 1518 (2004).

[41] Ni Yao, Quan Yao, Xiu-Ping Xie, Yang Liu, Peizhen Xu, Wei Fang, Ming-Yang Zheng, Jingyun Fan, Qiang Zhang, Limin Tong, and Jian-Wei Pan, Optimizing up-conversion single-photon detectors for quantum key distribution, Opt. Express **28**, 25123 (2020).

[42] Felix Mann, Helen M. Chrzanowski, Felipe Gewers, Marlon Placke, and Sven Ramelow, Low-noise quantum frequency conversion in a monolithic bulk ppktp cavity, Phys. Rev. Appl. **20**, 054010 (2023).

[43] Eric Bersin, *et al.*, Development of a Boston-area 50-km fiber quantum network testbed, ArXiv:2307.15696 (2023).

[44] C. T. Nguyen, D. D. Sukachev, M. K. Bhaskar, B. Machielse, D. S. Levonian, E. N. Knall, P. Stroganov, C. Chia, M. J. Burek, R. Riedinger, H. Park, M. Lončar, and M. D. Lukin, An integrated nanophotonic quantum register based on silicon-vacancy spins in diamond, Phys. Rev. B **100**, 165428 (2019).

[45] M. K. Bhaskar, R. Riedinger, B. Machielse, D. S. Levonian, C. T. Nguyen, E. N. Knall, H. Park, D. Englund, M. Lončar, D. D. Sukachev, and M. D. Lukin, Experimental demonstration of memory-enhanced quantum communication, Nature **580**, 60 (2020).

[46] L.-M. Duan and H. J. Kimble, Scalable photonic quantum computation through cavity-assisted interactions, Phys. Rev. Lett. **92**, 127902 (2004).

[47] Terry Rudolph, Why I am optimistic about the silicon-photonic route to quantum computing, APL Photonics **2**, 030901 (2017).

[48] Sara Bartolucci, Patrick Birchall, Hector Bombín, Hugo Cable, Chris Dawson, Mercedes Gimeno-Segovia, Eric Johnston, Konrad Kieling, Naomi Nickerson, Mihir Pant, Fernando Pastawski, Terry Rudolph, and Chris Sparrow, Fusion-based quantum computation, Nat. Commun. **14**, 912 (2023).

[49] Christophe Couteau, Stefanie Barz, Thomas Durt, Thomas Gerrits, Jan Huwer, Robert Prevedel, John Rarity, Andrew Shields, and Gregor Weihs, Applications of single photons to quantum communication and computing, Nat. Rev. Phys. **5**, 326 (2023).

[50] Nicolas Maring, *et al.*, A general-purpose single-photon-based quantum computing platform, ArXiv:2306.00874 (2023).

[51] Leo Yu, Chandra M. Natarajan, Tomoyuki Horikiri, Carsten Langrock, Jason S. Pelc, Michael G. Tanner, Eisuke Abe, Sebastian Maier, Christian Schneider, Sven Höfling, Martin Kamp, Robert H. Hadfield, Martin M. Fejer, and Yoshihisa Yamamoto, Two-photon interference at telecom wavelengths for time-bin-encoded single photons from quantum-dot spin qubits, Nat. Commun. **6**, 8955 (2015).

[52] Madison Sutula, Ian Christen, Eric Bersin, Michael P. Walsh, Kevin C. Chen, Justin Mallek, Alexander Melville, Michael Titze, Edward S. Bielejec, Scott Hamilton, Danielle Braje, P. Benjamin Dixon, and Dirk R. Englund, Large-scale optical characterization of solid-state quantum emitters, Nat. Mater. **22**, 1338 (2023).

[53] A. J. Stolk, *et al.*, Telecom-band quantum interference of frequency-converted photons from remote detuned nv centers, PRX Quantum **3**, 020359 (2022).

[54] Eric Bersin, Michael Walsh, Sara L. Mouradian, Matthew E. Trusheim, Tim Schröder, and Dirk Englund, Individual control and readout of qubits in a sub-diffraction volume, npj Quantum Inf. **5**, 38 (2019).

[55] V. Krutyanskiy, M. Galli, V. Krcmarsky, S. Baier, D. A. Fioretto, Y. Pu, A. Mazloom, P. Sekatski, M. Canteri, M. Teller, J. Schupp, J. Bate, M. Meraner, N. Sangouard, B. P. Lanyon, and T. E. Northup, Entanglement of trapped-ion qubits separated by 230 m, Phys. Rev. Lett. **130**, 050803 (2023).

[56] M. Pompili, S. L. N. Hermans, S. Baier, H. K. C. Beukers, P. C. Humphreys, R. N. Schouten, R. F. L. Vermeulen, M. J. Tiggelman, L. dos Santos Martins, B. Dirkse, S. Wehner, and R. Hanson, Realization of a multinode quantum network of remote solid-state qubits, Science **372**, 259 (2021).

[57] Maximilian Ruf, Noel H. Wan, Hyeongrak Choi, Dirk Englund, and Ronald Hanson, Quantum networks based on color centers in diamond, J. Appl. Phys. **130**, 070901 (2021).